Characterizing microstructures with representative tortuosities

Johan Chaniot, Maxime Moreaud, Loïc Sorbier, Pierre Marquet, Jean-Marie Becker, Thierry Fournel

Science and Technology for Energy Transition **79**, 31 (2024)

https://doi.org/10.2516/stet/2024023

Synthesis and characterisation of porous materials for clean energy applications
Nathalie Schildknecht and David Peralta (Guest Editors)

Available online at:
stet-review.org

REGULAR ARTICLE OPEN ACCESS

Characterizing microstructures with representative tortuosities

Johan Chaniot[1,2,4,*], Maxime Moreaud[4], Loïc Sorbier[4], Pierre Marquet[1,3,5,6], Jean-Marie Becker[2] and Thierry Fournel[2]

[1] CERVO Brain Research Center, Université Laval, 2601 Chemin de la Canardière, Québec, QC G1J 2G3, Canada
[2] Univ. Lyon, UJM-Saint-Etienne, CNRS, Institute of Optics Graduate School, Laboratoire Hubert Curien UMR5516, 42023 St-Etienne, France
[3] Department of Psychiatry and Neuroscience, Université Laval, Québec, QC, Canada
[4] IFP Energies nouvelles, Rond-point de l'échangeur de Solaize, BP 3, 69360 Solaize, France
[5] Centre d'optique, photonique et laser, Université Laval, 2375 rue de la Terrasse, Québec, QC, G1V 0A6, Canada
[6] Joint International Research Unit between Université Laval, Québec, QC, Canada and Centre for Psychiatric Neuroscience, Department of Psychiatry, Lausanne University Hospital and University of Lausanne, Prilly, Switzerland

Received: 24 October 2023 / Accepted: 29 March 2024

Abstract. This paper addresses the numerical characterization of microstructures by the concept of tortuosity. After a brief review of geometric tortuosities, some definitions are considered for a benchmarking analysis. The focus is on the *M-tortuosity* definition, which is revised by expliciting the link to percolation theory, among other things. This operator fits with the analysis of real samples of materials whatever their complexity. A contribution of this paper is a new formulation of the *M-tortuosity*, making it generic to many situations. Additionally, the comparison of the various tortuosimetric descriptors, state-of-the-art definitions and *M-tortuosity*, is proposed by considering several scenarios thanks to stochastic multi-scale models of complex materials. The relationships with porosity, morphological heterogeneity and structural anisotropy are investigated. The results highlight the similarities and differences between the descriptors while attesting that the *M-tortuosity* is equivalent to the state-of-the-art definitions, for a potential use in diffusion and conductivity analyses. Moreover, the *M-tortuosity* handles correctly situations where state-of the-art algorithms fail. The anisotropic case highlights some limitations of the state-of-the-art definitions behaving differently according to the given propagation direction. In the case of unknown propagation and irregular piece of materials, the *M-tortuosity* provides a unique tortuosity value representative of the whole microstructure while detecting the anisotropy. These operators are freely available within the *plug im!* platform.

Keywords: Microstructure, Materials science, Porous network, Morphological analysis, Mathematical morphology, Topology, Connectivity, Tortuosity, Geodesic distance transform, Percolation, Boolean model, Anisotropy, Heterogeneity.

Notations and vocabulary

The vocabulary used in the article is explicitly given. Knowing the confusion in the literature about geometric, geodesic or morphological tortuosities, it is necessary to clearly define the terms used in this article. Hereafter, the term geometric is chosen to qualify the tortuosity assessed by means of geodesic and Euclidean distance transforms.

The article defines notations and groups them based on their referents to improve readability. First, the notations associated with microstructures:

X: the porous microstructure,
l, w and h: primary grain parameters defining a platelet, used for simulating microstructures with a Boolean model,
V_v: volume fraction of primary grains of a homogeneous Boolean model,
V_a, R_a, V_i and V_o: heterogeneous Boolean model parameters formed of spheres, named aggregates, with different volume fractions of grains inside and outside,
n_r: number of realization of a model of microstructure,
σ: standard deviation of measurements over the n_r realizations,
l_σ: confidence intervals of measurements over the n_r realizations.

* Corresponding author: johan.chaniot.1@ulaval.ca

Notations for distance:

D_E: Euclidean distance,
D_G: geodesic distance,
L: Euclidean distance between two opposite planes of digitalized cubes of materials,
$D_E(p_m, p_n)$: value of the Euclidean distance map at point p_m from p_n,
$D_G(p_m, p_n; X)$: value of the geodesic distance map in X at point p_m from p_n,
$V_D(n)$: volume of the direct reconstruction of X at step n,
$V_G(n)$: volume of the geodesic reconstruction of X at step n.

Notations for tortuosity:

τ: geometric tortuosity of a path,
τ_g: geometric tortuosity of X considering the minimal geodesic path between two opposite planes,
τ_m: geometric tortuosity of X considering the mean value of the geodesic paths between two opposite planes,
τ_P: geometric tortuosity of X considering the Peyrega et al. definition,
τ_B: geometric tortuosity of X considering the Berrocal et al. definition,
τ_G: geometric tortuosity of X considering the Gommes et al. first definition,
τ_{G_r}: geometric tortuosity of X considering the Gommes et al. second definition.

Notations for *M-tortuosity*:

S_1: a set of points p_n in X,
S_{2_n}: a set of points associated to p_n.
$\tau_{n,m}$: geometric tortuosity between the two points p_n and p_m of X,
L_n: local insight of X from p_n,
T: representative tortuosity or *M-tortuosity* of X.

1 Introduction

Structural analysis of materials is a common issue in materials science, being of particular interest since connections have been highlighted between the structure and the physicochemical parameters of these materials, especially for porous media [1–3]. Among the usual concepts used for characterization purposes, tortuosity [4] lies on a central position in materials science [5–7]. Tortuosity has been reviewed many times from distinct perspectives. Clennell [5] presents the first exhaustive review focusing on physical meanings. Ghanbarian *et al.* [7] propose an update while discussing the relationship with percolation theory. Fu *et al.* [6] describe the various algorithms for physical assessment of tortuosity. Among the various notions extracted from the concept of tortuosity, the geometric tortuosity has a central position, having the potential to be used in numerous applications dealing with transport properties of materials, such as diffusion analysis [8, 9]. The geometric tortuosity is connected to several concepts such as percolation, connectivity, sinuosity and constrictivity [10–12].

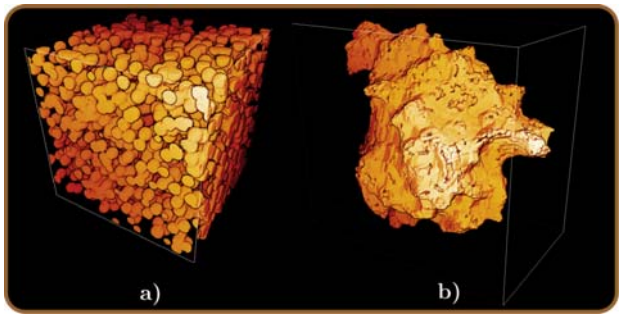

Fig. 1. Microstructures illustrations. (a) Boolean schemes of spheres generated in a cube where straightforward definition of propagation direction for tortuosity calculations is possible. (b) real γ-alumina sample, imaged by electron tomography (resolution around 1 nm·vx^{-1}, *vx* standing for voxel), where a proper propagation direction is delicate to define. Volume (a) was generated using [35] and volumes (a) and (b) were rendered using [35].

In practice, the aim is to extend geometric tortuosity from a single pore to the characterization of the entire microstructure. The flow under consideration is often assumed to propagate in a given direction, simplifying the analysis of the microstructure as a whole. Therefore, such a tortuosity appears to be a well-suited notion for characterizing digitalized cubes of materials (see Fig. 1a). Nevertheless, its implementation required some adaptations in cases as irregular pieces of materials as γ-alumina samples [13] (see Fig. 1b), for which the definitions in the literature are not applicable.

The *M-tortuosity* was introduced as an efficient and fast way breaking free directional aspects of previous approaches to address the challenge by stochastically probing microstructures [14, 15]. The *M-tortuosity* answers practically to the requirement of application to any complex microstructures as the microstructure presented in Figure 1b. Nevertheless, a practical need of versatility subsists for this descriptor in reflecting more or less some microstructural properties, especially those related to percolation and sinuosity. Furthermore, no study has discussed the relevance of *M-tortuosity* for practical purposes, unlike the standard definitions used in various applications [8, 9, 16]. Additionally, there are no articles that compare the chosen classical approaches with each other.

Consequently, our contribution is a novel version of the *M-tortuosity* definition. We introduce new parameters that promote or inhibit geodesic paths based on their length and eccentricity. We propose an alternative version of the *M-tortuosity* that uses arithmetic means instead of harmonic means, simplifying the original formulation. These novel definitions ensure proper disconnection handling. Furthermore, our new perspective on microstructure analysis is compared to state-of-the-art definitions, as shown in Figure 2. This positions our descriptor in relation to others while emphasizing its potential for analyzing transport properties in atypical contexts. Finally, to the best of our knowledge, this is the first time that different purely morphological definitions of tortuosity are compared.

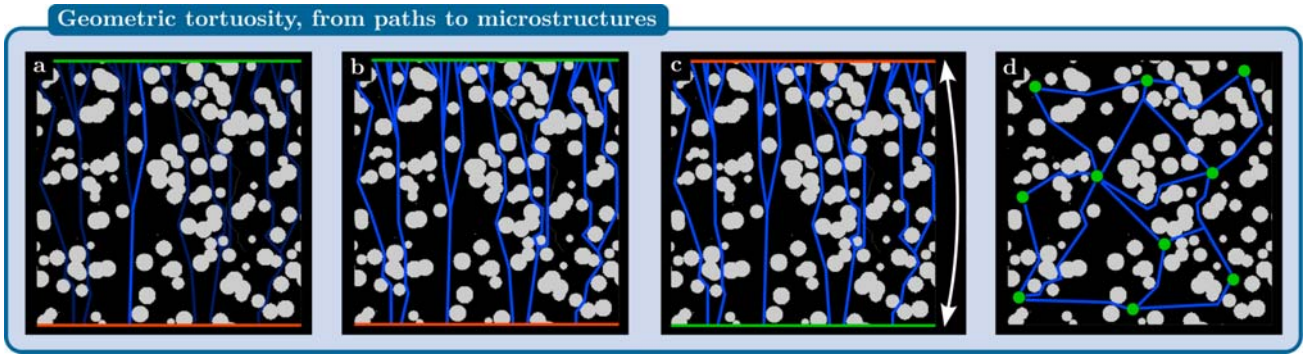

Fig. 2. Strategies to extend geometric tortuosity from paths to microstructures. Illustrations of various ways to characterize whole microstructures based on geometric tortuosity definition (Eq. (8)). (a) path of minimal length connecting entry (green) and exit (red) planes (Eq. (2)), (b) average of paths connecting entry and exit planes (Eq. (3)), (c) point tortuosities, *i.e.*, tortuosity map, assessed by forward and backward propagations between two opposite planes (Eq. (4)), (d) *M-tortuosity* averaging local tortuosities between random locations.

In this article, state-of-the-art definitions of tortuosity are briefly recalled, all based on the definition of the geometric tortuosity making use of well-known concepts as accessibility, connectivity and sinuosity. The original definition of the *M-tortuosity* is defined and its extension is proposed in the following section, after discussing limitations and challenges related to standard tortuosities. In the results and discussion section, stochastic multi-scale microstructure models of binary materials are considered and analyzed to compare the different tortuosimetric descriptors. The *M-tortuosity* behaves similarly to the other definitions when faced to the evolution of morphological features as volume fraction, making it a potential equivalent of the latter when they do not fit to the material to be analyzed.

2 Tortuosities

Geometric tortuosity is based on several well-known concepts in numerical characterization of materials. Accessibility is described by the percolation theory, as it assesses the existence of a path, fully included in the microstructure, connecting two regions, usually the entry and the exit. Connectivity follows accessibility and focuses on quantifying the degree of interconnection of the network, *i.e.* the microstructure. Usually, the Euler number, or the Euler-Poincaré feature, is considered to assess connectivity. Sinuosity is the last notion involved in tortuosity, evaluating how sinuous a path is, which could be seen as the integral of the local curvature along the path.

2.1 Morphological insights in material science

Geometric tortuosity characterization consists in assessing the impact of a microstructure's morphology over percolating paths. Originally, geometric tortuosity is defined for a path, *i.e.*, a pore, connecting two specific locations, entry and exit, then focusing on sinuosity only [17]. The definition used in [18], based on rotation-invariant operators such as distance transforms, is defined as the ratio of the geodesic distance, *i.e.*, constrained path, by the Euclidean distance between the entry and the exit. In other words, the geometric tortuosity of a unique pore is the normalization of the geodesic distance by the Euclidean distance,

$$\tau = \frac{D_{\mathrm{G}}}{D_{\mathrm{E}}}. \tag{1}$$

Consequently, the issue to address is how to extend this local definition in order to characterize a whole microstructure X with its sinuosity and connectivity. Decker *et al.* [18] proposes to analyze the probability distribution function of the geodesic distances over the network between parallel faces. The issue of reducing this distribution to a scalar value is then addressed.

The first idea is to assess the minimal geodesic distance of a constrained path starting from an entry, a plane for instance, to the exit, the opposite plane, normalized by the Euclidean distance between the two planes L (see Fig. 2a). In this case, a propagation direction is clearly defined,

$$\tau_{\mathrm{g}} = \frac{\min\{D_{\mathrm{G}}\}}{L}, \tag{2}$$

with D_{G} the geodesic distance map at the exit plane.

Nevertheless, considering only the minimal path can be too restrictive; computing the average is more representative of the microstructure, giving rise to this second definition (see Fig. 2b),

$$\tau_{\mathrm{m}} = \frac{\mathrm{mean}\{D_{\mathrm{G}}\}}{L}. \tag{3}$$

These previous definitions take implicitly pore width into consideration, *i.e.*, two very similar pores, one being a slightly bigger version of the other, have distinct tortuosity as shown in Figure 3. The use of homothopic skeleton $\mathcal{S}k$ [19], defining geometric tortuosities according to Stenzel *et al.* [16] in contrast to geodesic tortuosities computed over the "transporting phase", leads to invariance with respect to the scale or to the size of a moving particle percolating through the porosity (see Fig. 3). Moreover, the skeleton

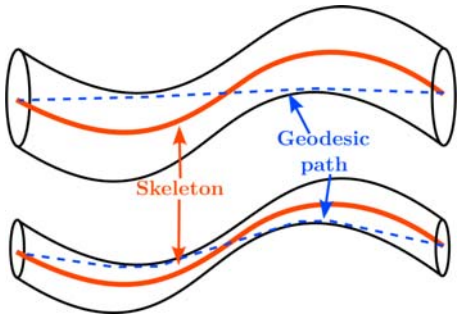

Fig. 3. Geodesic paths according to the pore width. Illustrations of the dependency of the geodesic path (blue dashed lines) to the pore width, contrary to the skeleton (orange lines) being the same for the two pores despite their distinct width.

provides a less scattered distribution of distances, as shown in [14].

However, no map of tortuosity can be extracted explicitly from these definitions. Indeed, if we consider the geodesic map of the whole structure divided by L, only the values of the exit plane correspond to proper tortuosity values. Peyrega *et al.* [20] propose a distinct definition, considering forward propagation from a plane A and backward propagation from an opposite one B (see Fig. 2c), in order to provide tortuosity of each point p of the microstructure,

$$\tau_{\mathrm{P}}(p) = \frac{D_{\mathrm{G}_{A\to B}}(p) + D_{\mathrm{G}_{B\to A}}(p)}{L} \tag{4}$$

with $D_{\mathrm{G}_{A\to B}}$ the geodesic distance map in the direction A toward B, A being the entry or the source plane.

This definition increases the amount of information while providing a tortuosity map, analyzed by means of histograms for each of the three propagation directions. This tortuosity map has the advantage to be constrained by the orientation only, *i.e.*, the axis, as forward and backward propagations are performed.

However, these definitions of tortuosity based on a propagation direction between opposite planes and an approximation of the Euclidean distance (L), are sensitive to relative deviation. In other words, a tortuosity higher than 1 will be attributed to a straight leaning pore, whose tortuosity value will depend on the angle of inclination with respect to the propagation direction. In order to tackle this issue, a return to point definition seems necessary, which is done in the following definition.

In fracture analysis, Berrocal *et al.* [21] propose to weight the tortuosity of a fracture, *i.e.*, a path, by the geodesic distance in order to gather several tortuosities in a final mean value promoting sinuous paths. The consideration of the original definition (Eq. (8)) leads to invariance with respect to relative deviation.

$$\tau_{\mathrm{B}} = \mathrm{mean}\{D_{\mathrm{G}} \cdot \tau\}. \tag{5}$$

Distinct interpretations of tortuosity have been proposed in [22], considering a propagation direction between opposite planes but the real Euclidean distance D_{E}. Tortuosity is first seen as the limit toward infinity of the original ratio (Eq. (8)),

$$\tau_{\mathrm{G}} = \lim_{D_{\mathrm{G}}\to\infty} \frac{D_{\mathrm{G}}}{D_{\mathrm{E}}}. \tag{6}$$

Practically, τ_{G} is assessed by the initial slope of a parabolic fit of D_{G} *vs.* D_{E}, both computing from a source plane. A second definition considers morphological reconstruction, direct and geodesic, to define tortuosity as a ratio of volumes; volume of the direct reconstruction V_{D} by volume of the geodesic reconstruction V_{G},

$$\tau_{\mathrm{G}_r} = \lim_{n\to\infty} \frac{V_{\mathrm{D}}(n)}{V_{\mathrm{G}}(n)} \tag{7}$$

with n the step in the reconstruction processes.

The main advantage of this second definition where Euclidean and geodesic quantities are reversed to provide a value upper than 1 [23], is its straightforward extension to gray-scale images, avoiding a delicate step of segmentation. These definitions give access to tortuosity maps too, as geodesic and Euclidean values are computed for each point, but constrained by the propagation direction.

Consider the primary application target of this article: the 3D images of irregular samples of real materials, such as the one presented in Figure 1b. Directional definitions are not adapted to this kind of images, samples being too small to extract a representative cube from them. To this end, a pore-to-pore tortuosity map is proposed by Moreaud *et al.* [24], by identifying the different entries of the porous microstructure, to assess the material's accessibility while extracting tortuosity matrices quantifying each entry in relation to the others.

2.2 Limitations and challenges

Despite these various definitions, none can be applied on both microstructures of Figure 1: digitalized cubes of materials and irregular small samples of materials. In the context of characterizing the microstructure of Figure 1b, only the definition of [24] can be used for practical purposes, but cannot be compared to the other definitions which are commonly used in physicochemical analyses. Recently, the *M-tortuosity* overcomes this issue (see Fig. 2d) [14], providing the ability of characterizing irregular samples of real materials to reach internal nanometric porosity analysis, as shown by Batista *et al.* [25]. In contrast to the state-of-the-art definitions presented above, the *M-tortuosity* is the only definition applicable on both microstructures of Figure 1. In what follows, we first recall the original definition of *M-tortuosity*, before proposing an extended definition of this notion.

3 *M-tortuosity*; original definitions

Initially, the *M-tortuosity* has been defined to overcome the complexity of materials such as γ-alumina sample in Figure 1b [14, 25], by probing the microstructure in random directions and at various scales. Its principle is the following; several locations are probed, their local insights are gathered into a final representative viewpoint of the whole microstructure. In the literature, the *M-tortuosity* and the

H-tortuosity are defined, providing scalar value and curve as final representative viewpoint of the microstructure, respectively. Both are based on the same mathematical formulation [14, 15].

3.1 Stochasticity for complexity overcoming

If we consider the material of Figure 1b, entry and exit planes are not available. To overcome this pitfall, a random drawing of locations, *i.e.* points inside the microstructure X, is considered [26]. The N probed locations are defined randomly through a stratified sampling, ending to the points set definition $S_1 = \{p_n\}_{n\in[[0,\,N-1]]}$. Consequently, the tortuosity is computed between points instead of planes. Considering two connected points in X p_n, the source point, and p_M, the tortuosity is,

$$\tau_{n,m} = \frac{D_G(p_m, p_n; X)}{D_E(p_m, p_n)} \tag{8}$$

with $D_E(p_m, p_n)$ the value of the Euclidean distance map at point p_m from p_n, and $D_G(p_m, p_n; X)$ the value of the geodesic distance map in X at point p_m from p_n. For brevity, $D_{G_{n,m}} = D_G(p_m, p_n; X)$ and $D_{E_{n,m}} = D_E(p_m, p_n)$.

3.2 Second set and tortuosity dimension

The local insights are based on S_2 a collection of sets of points, each assigned to a point $p_n \in S_1$, $S_2 = \{S_{2_n}\}$ and $p_m \in S_{2_n}$. For the *M-tortuosity*, $S_{2_n} = S_1 \backslash \{p_n\}$ giving rise to a scalar local insight L_n (the *M-coefficient* in [14]). For the *H-tortuosity*, $S_{2_n} = \{S_d\}_{d\in[[0,\,D-1]]}$ with $S_d = \{p_m; d < D_E(p_m, p_n) \leq d+1, d \in \mathbb{N}^*\}_{m\in[[0,\,M-1]]}$ representing the surrounding neighborhoods of p_n as a function of the Euclidean distance d, M being the number of accessible points located at a distance of d from p_n, leading to a curve as local insight L_n (the *H-coefficients* in [15]).

In other words, for each p_n, the *M-tortuosity* considers the geodesic paths to all the other points of S_1, whereas the *H-tortuosity* simulates a wave propagating from p_n in the microstructure. These local insights L_n are then gathered into the final representative tortuosities T (*M-scalar* or *H-scalars*), which keeps the dimension of L_n.

3.3 Weighted averages

The local insights L_n and the final representative tortuosities T are defined by weighted average, more specifically the harmonic mean, defined by the reciprocal of the arithmetic mean of the reciprocals of the values, which is an ideal candidate for disconnections handling as well as isolation. Disconnection arises when no path in X exists between two given points, and the geodesic distance of two non-connected points of X is infinite. With harmonic mean these two points do not interfere in the computation, leading to zero contribution. Isolation is the extension of disconnection and arises when there exists no point in a subset S_{2_n} connected to a given point p_n.

The weights considered in L_n and T both promote certain geodesic paths of the whole microstructure. Consequently, the point tortuosities values $\tau_{n,m}$ in L_n are weighted by the corresponding geodesic distance $D_{G_{n,m}}$, and the L_n values in T are weighted by the Euclidean distance between p_n and p_c, the center of inertia of X. The latter weighting is based on the following idea, the eccentricity of p_n is connected to the representativity of its local insight L_n.

3.4 Alternative definitions

To improve the computational efficiency, a graph-based definition is given to the *M-tortuosity* by Hammoumi *et al.* [27]. Deterministic definitions are proposed in [25] by imposing S_1 and S_2 to meet the specific application goal of this article. S_1 is composed of the centers of inertia p_n of particles inside the porous medium and $S_{2_n} = S_1 \backslash \{p_n\}$, leading to analyze the relative locations of particles with respect to the microstructure constraint. Finally, the *A-protocol* defined in [28] and embedded the *M-tortuosity*, gives rise to accessibility consideration by simulating a probe of given size travelling through the network [14, 15].

4 *M-tortuosity*; extended definition

M-tortuosity and *H-tortuosity* are gathered into a single manifold tortuosity called *M-tortuosity*. This extended definition is enriched of new parameters, correcting some issues in the original definition while increasing the versatility. The first parameters named α allow to reach proper promotion of long geodesic paths among other things and provide the user the opportunity to adapt the definition to its own application by controlling the promotion of certain paths. The second parameters, named ρ and embedding percolation, lead to proper disconnection and isolation insensitivity, which is a major distinction with the state-of-the-art definitions. Consequently, we consider the arithmetic mean as an alternative to the harmonic one. Both are defined.

4.1 Local insights

M-tortuosity versatility relies on S_1 and S_2 definition. S_2 has a key role in the very meaning of the resulting descriptor, its structure inducing the type of the operator, as shown above. Formally speaking, the collection S_2 is a set of rank s defining the dimension of the local insights being equal to $s-2$. This rank to three, resulting in a local insight of dimension one or zero, fitting with the literature definitions.

Consequently, keeping the previous notations, $S_{2_n} = \{S_d\}$ and $S_d = \{p_m\}$ but d is no longer necessarily a distance, for generalization purposes. For $n \in [[0,\, N-1]]$, local insights set L_n attached to each $p_n \in S_1$ are defined as a function of d using the harmonic or the arithmetic mean of the geometric tortuosities between p_n and each p_m. Then, for all $d \in [[0,\, D-1]]$, using the harmonic mean,

$$L_{n_H}^{-1}(d) = W_{1H_n} \cdot \left(\sum_{m=0}^{M-1} \rho_{1_{n,m}} \cdot D_{G_{n,m}}^{-\alpha_1} \cdot \tau_{n,m}^{-1} \right)^{-1} \tag{9}$$

with,

$$W_{1H_n} = \sum_{m=0}^{M-1} \rho_{1_{n,m}} D_{\mathrm{G}_{n,m}}^{-\alpha_1} \tag{10}$$

and using the arithmetic mean,

$$L_{n_A}(d) = W_{1A_n}^{-1} \cdot \left(\sum_{m=0}^{M-1} \rho_{1_{n,m}} \cdot D_{\mathrm{G}_{n,m}}^{\alpha_1} \cdot \tau_{n,m} \right) \tag{11}$$

with,

$$W_{1A_n} = \sum_{m=0}^{M-1} \rho_{1_{n,m}} D_{\mathrm{G}_{n,m}}^{\alpha_1}. \tag{12}$$

The power factor parameter $\alpha_1 \in \mathbb{Z}$ is one of the additional parameters, modifying the original weighting; the larger $|\alpha_1|$, the more the longest ($\alpha_1 > 0$) or shortest ($\alpha_1 < 0$) geodesic paths are promoted with the arithmetic definition (to be reversed with harmonic definition). The Boolean matrix ρ_1 allows to reach the disconnections insensitivity. $\rho_{1_{n,m}}$ is equal to 1 if and only if there exists a path connected $p_n \in S_1$ to $p_m \in S_2$.

4.2 Representative tortuosity

The representative viewpoint T of the whole microstructure is defined for all $d \in [\![0,\ D-1]\!]$, considering p_c and the second power factor $\alpha_2 \in \mathbb{Z}$, by

$$T_H(d) = W_{2H_n} \cdot \left(\sum_{n=0}^{N-1} \rho_{2_n} D_{\mathrm{E}_{c,n}}^{-\alpha_2} \cdot L_{n_H}(d) \right)^{-1} \tag{13}$$

with,

$$W_{2H_n} = \sum_{n=0}^{N-1} \rho_{2_n} D_{\mathrm{E}_{c,n}}^{-\alpha_2} \tag{14}$$

if the harmonic mean is considered, and if the arithmetic one is used, by,

$$T_A(d) = W_{2A_n}^{-1} \cdot \left(\sum_{n=0}^{N-1} \rho_{2_n} D_{\mathrm{E}_{c,n}}^{\alpha_2} \cdot L_{n_A}(d) \right) \tag{15}$$

with,

$$W_{2A_n} = \sum_{n=0}^{N-1} \rho_{2_n} D_{\mathrm{E}_{c,n}}^{\alpha_2}. \tag{16}$$

The second power factor α_2 extends the original definition, the latter corresponding to $\alpha_2 = 1$; the larger $|\alpha_2|$, the more the furthest ($\alpha_2 > 0$) or nearest ($\alpha_2 < 0$) points from p_c are promoted with the arithmetic definition (to be reversed with harmonic definition). The Boolean vector ρ_2 allows to reach the isolations insensitivity. ρ_{2_n} is equal to 1 if and only if there exists a path connected $\rho_n \in S_1$ to any $\rho_m \in S_2$.

This new formulation gathers the previous definitions. For a scalar analysis, S_{2_n} is a points set, then $d = \{0\}$ and $S_{2_n} = S_d = S_1 \backslash \{p_n\}$. For curve analysis, S_{2_n} is a collection of sets of points, then $d > 0$ and $S_{2_n} = \{S_d\}_{d \in [\![0,\ D-1]\!]} = \{\{p_m\}_{m \in [\![0,\ M-1]\!]}\}_{d \in [\![0,\ D-1]\!]}$. In the case of [15], d is a distance, D is the maximal distance from each source point for microstructure probing, and M is the number of points in X accessible from a given source point p_n of S_1 and located at distance d from it.

4.3 Versatility for broad applications

In the original definition, the isolation insensitivity was not properly reached. The weight at the numerator associated to an isolated point $p_n \in S_1 (L_n = 0)$ is still taken into account. This statement suggests that the *M-tortuosity* is sensitive to isolation. ρ_{2_n} fixes this issue by being equal to 1 if and only if p_n is not isolated. Our contribution improves the versatility of the *M-tortuosity* thanks to two additional parameters pairs, denoted as $(\rho_{1_{n,m}}, \alpha_1)$ and (ρ_{2_n}, α_2), while preserving the benefits of the original definitions. The first element of each pair highlights the consideration of percolation using Boolean values and the second element being power factors serving for path length and excentricity promotions, respectively. This novel definition is properly insensitive to disconnections and to isolations. To highlight the increase of verstatility, two aspects are discussed.

First, let consider Figures 1a and 1b. In the case of scalar tortuosimetric characterization, by imposing $\alpha_2 > 0$, long geodesic paths are promoted a second time as points closer to the image boundaries have a higher probability to get longer geodesic paths in their local insight than points close to p_c. In contrast, in case of characterization using tortuosity curves, $\alpha_2 < 0$ promotes points closer to p_c being less impacted by the boundary effect. As a conclusion, the α_2 value allows to fit with the application.

Second, the harmonic mean provides lower values than the arithmetic one. The choice between the two means can be motivated by the application. Indeed, the harmonic mean, usually used when rates and ratios are involved, brings us closer to the acoustic tortuosity definition [29, 30]. Indeed, distance values can be interpreted as time values instead of spatial values.

5 Results and discussion

This section deals with binary microstructures analysis by means of tortuosimetric numerical operators, focusing on scalar characterization only. Moreover, all computations are performed over the whole microstructure, without skeleton preprocessing. First, the *M-tortuosity* is analyzed and the harmonic and arithmetic definitions are compared while the impact of the parameters (α_1, α_2) is assessed. Second, the comparison to the classical descriptors is performed on synthetic microstructures. The synthetic microstructures are generated from random model as described below.

5.1 Random models of porous microstructures

Boolean models generates homogeneous microstructures, *i.e.*, structure possessing a unique scale of grains' density, made of isotropic or anisotropic grains A', located at Poisson points [31]. They are defined by a single volume

fraction of grains V_v and by the grains' morphology. In order to analyze heterogeneity, multi-scale microstructures are generated by using Cox models [32, 33], providing materials with aggregates or inclusions, *i.e.*, areas of higher or lower density of grains. In the following, two-scale models are defined by three volume fractions: V_a the volume fraction of aggregates, V_i and V_o, the volume fraction of grains inside and outside the aggregates, respectively. Aggregates are defined as spheres of radius R_a. A unique grain's morphology is considered for the homogeneous and heterogeneous cases, the platelet shape [34], being defined by three parameters, length l, width w and height h, all equal to 10 (units are in pixels). For each model, 40 realizations, *i.e.*, volumes, of size 400^3 are generated. Figures 4a and 4b show the shapes of the platelets and the aggregates, respectively.

Tortuosity as a function of the volume faction of homogeneous microstructures is first considered; 3 models ((1)–(3)) are generated, represented by the three first columns in Table 1 (Fig. 4, two first microstructures). Second, aggregation impact on tortuosity is assessed by two additional heterogeneous microstructures, named (4) and (5), represented by the two last columns in Table 1 (Fig. 4, third microstruture). The homogeneous models are then transformed into anisotropic models, named (1'), (2') and (3'), by simulating a compression of the materials in the x direction by the suppression of one plane over two (Fig. 4, last microstruture).

Figure 4 illustrates the models by displaying the shapes of grains and aggregates, together with some realizations of the models, volumes and slices, highlighting the considered situations: increasing of volume fraction of grains V_v, increasing of the heterogeneity and impact of the anisotropy. The complementary set of the grains set represents the porosity (black areas in Fig. 4). Let V_p be the porous volume fraction, being define in the homogeneous case by $V_p = 1 - V_v$.

Confidence intervals with 95% confidence level are equal to $l_\sigma = 2\sigma/\sqrt{n_r}$ with σ the standard deviation over the n_r realizations. Finally, in this case, the tortuosimetric analysis provides averaged assessments. Let $\tau(M)$ be a given descriptor value for a given model (M), $\tau(M)$ is the averaged value over all realizations of the set of tortuosity values of each realization.

5.2 *M-tortuosity*

Considering the *M-tortuosity*, the focus is on the scalar version of the representative tortuosity, named T_{α_1,α_2}, by defining $S_{2_n} = S_1 \backslash \{p_n\}$ and S_1 being drawn randomly by a stratified stochastic process as in [14]. The impacts of (α_1, α_2), as well as the choice of the mean, are analyzed; $\alpha_1 = \alpha_2 = \{-10, -5, -2, -1, 0, 1, 2, 5, 10\}$. The models (3) is considered in Figure 5, for these purposes.

As expected, the harmonic version of the *M-tortuosity* (Fig. 5a) provides slightly smaller values than the arithmetic one (Fig. 5b), but this difference is negligible when compared to the differences with the state-of-the-art definitions. Moreover, the impacts of α_1 and α_2 are reversed between the harmonic and the arithmetic definitions. When α_1 tends towards infinity the long geodesic paths are promoted in the arithmetic *M-tortuosity* (short geodesic paths with the harmonic *M-tortuosity*), which is reversed if α_1 tends towards minus infinity. When α_2 tends towards infinity the source points the furthest of p_c are promoted (the nearest of p_c with the harmonic *M-tortuosity*), which is reversed if α_2

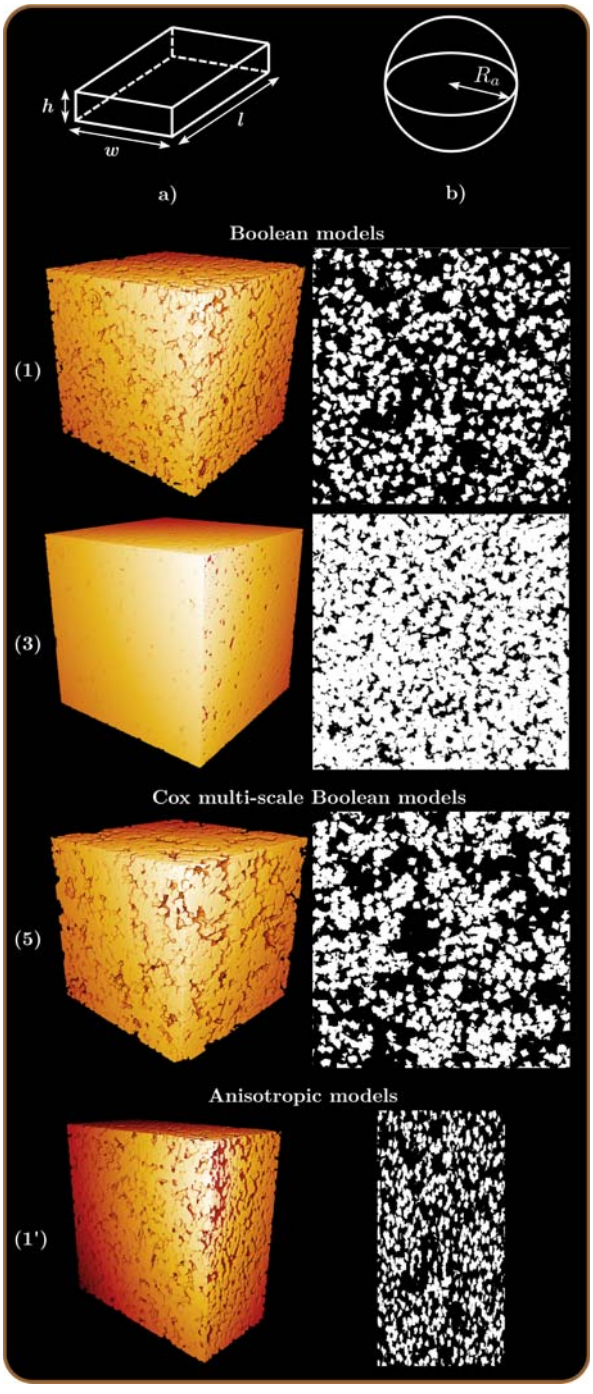

Fig. 4. Synthetic microstructures illustrations. (a) The grains shape (cubic platelet) and (b) the aggregate shape. Volume representation and 2D slice of a realization of Boolean models presenting the two isotropic cases, homogeneous: (1) $V_v = 0.4$ and (3) $V_v = 0.6$, and heterogeneous: (5) $V_i = 0.65$ and $V_o = 0.15$, and the anisotropic case: (1') $V_v = 0.4$. Volumes and slices generated and rendered using [35].

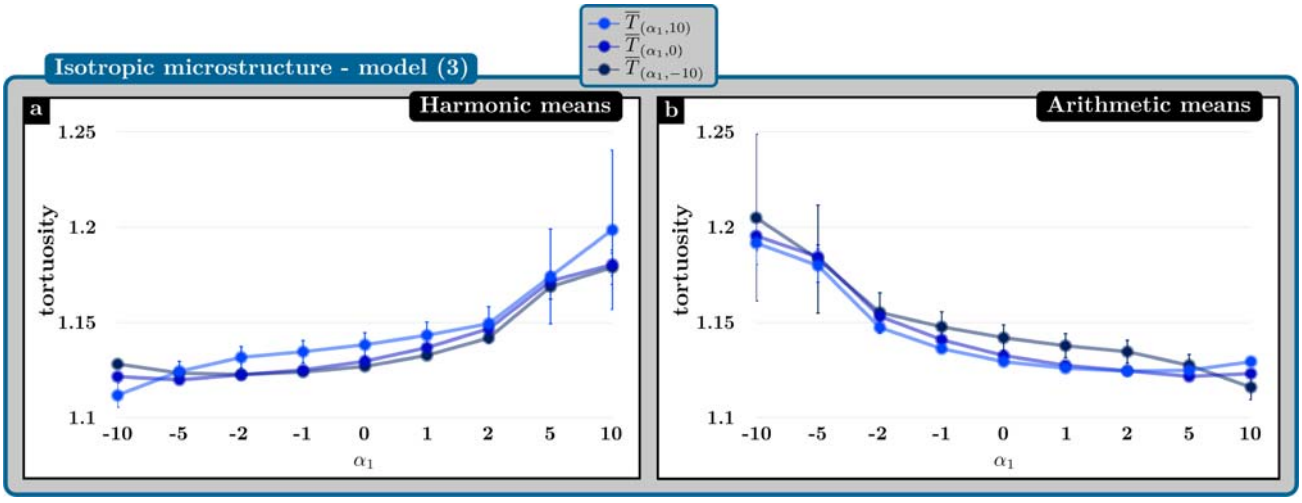

Fig. 5. *M-tortuosity* as a function of α_1 and α_2. Average *M-tortuosity* values with their corresponding confidence intervals l_σ, computed on 40 realizations of model (3). Screening of parameters $\alpha_1 = \{-10, -5, -2, -1, 0, 1, 2, 5, 10\}$ and $\alpha_2 = \{-10, 0, 10\}$. (a) Harmonic means representative tortuosities T_{H}. (b) Arithmetic means representative tortuosities T_A.

Table 1. Synthetic microstructures parameters. Boolean models generated using [35]; (1), (2) and (3) are one-scale models, considered to assess the impact of volume fraction, and (4) and (5) are two-scales models, considered to assess the impact of aggregation or morphological heterogeneity, both over tortuosimetric measurements.

Models	(1)	(2)	(3)	(4)	(5)
V_v/V_i	0.4	0.6	0.8	0.57	0.65
V_o				0.23	0.15
V_a				0.5	0.5
R_a				20	20

tends towards minus infinity. Globally, the short geodesic paths promotion makes increase the tortuosity, but the confidence interval l_σ too. This comment is in good agreement with the results of Chaniot *et al.* [15], who highlight that larger tortuosities are obtained for short paths.

For the rest of the analysis, we will considered the arithmetic *M-tortuosity* only.

5.3 Tortuosimetric analysis

Some definitions are adapted to perform the comparison analysis. All definitions considered are presented in Table 2. Equations (2) and (3) are unchanged. Considering the definition of Peyrega *et al.* [20] (Eq. (4)), the mean over the tortuosity map provides the final scalar value used hereafter. The weighted tortuosity (Eq. (5)), of which the weighting is considered in the *M-tortuosity* definition, is adapted to plane to plane propagation. The computational processes of Gommes *et al.* [22] are used for ending on scalar values. The definition of Moreaud *et al.* [24] is not considered as it is not adapted to this comparison analysis. The state-of-the-art tortuosities is computed in the x, y, z directions and their arithmetic mean is used for comparison with the *M-tortuosity* (Fig. 6).

Table 2. Tortuosities. List of the tortuosity definitions: reference plane-based tortuosities (τ_{g} and τ_{m}), plane-based tortuosities (τ_{B}, τ_{P}, τ_{G} and τ_{G_r}) and stochastic tortuosities ($T_{A(\alpha_1,\alpha_2)}$).

Tortuosity name	Symbol	Equation
Minimal	τ_{g}	(2)
Mean	τ_{m}	(3)
Forward/backward	τ_{P}	(4)
Weighted mean	τ_{B}	(5)
Limit	τ_{G}	(6)
Morphological reconstruction	τ_{G_r}	(7)
Arithmetic *M-tortuosity*	$T_{A(\alpha_1,\alpha_2)}$	(15)

Tortuosities are separated into two groups: the definitions based on propagation direction definition, named plane-based tortuosities, and the arithmetic *M-tortuosity* based on stochastic points process (see Table 2). The two original definitions of tortuosity making use of minimal geodesic path τ_{g} and averaging geodesic paths τ_{m} are used as arbitrary reference. Four scenarios are considered: in the case of isotropic microstructures, the impacts of decreased V_p and of increased heterogeneity, and in the case of anisotropic microstructures, the impacts decreased V_p and of structural anisotropy at constant V_p. Tortuosity behaviors are evaluated and the various approaches are compared in Figure 6. Tortuosity values are given in Tables 3 and 4. For the sake of brevity, we only provide the necessary values to support our statements. Confidence intervals are sometimes too small to be clearly visible, attesting the representativity of the results.

5.3.1 *Isotropic microstructures*

Figures 6a and 6b present the behavior of tortuosity with the decreasing of the porous volume fraction V_p and with the increasing of heterogeneity, respectively.

Table 3. Tortuosities of microstructures. Average tortuosities with the corresponding standard deviation std, computed on 40 realizations of each model. Models (1), (2) and (3) assess the impact of volume fraction. Models (4) and (5) assess the impact of heterogeneity. Models (1'), (2') and (3') assess the impact of anisotropy; all propagating direction are evaluated, x (compression direction) and y (perpendicular direction) are displayed as well as the mean value (mean) over the three spatial directions.

	Tortuosity					
Model	τ_g l_σ	τ_m l_σ	τ_B l_σ	τ_P l_σ	τ_G l_σ	τ_{G_r} l_σ
(1) Mean	1.0178	1.0444	1.0444	1.0471	1.0511	1.0500
	0.0006	0.0001	0.0001	0.0001	0.0002	0.0003
(2) Mean	1.0525	1.0855	1.0855	1.0892	1.0936	1.0945
	0.0007	0.0002	0.0002	0.0002	0.0004	0.0006
(3) Mean	1.1334	1.1872	1.1875	1.1891	1.1951	1.2049
	0.0013	0.0009	0.0009	0.0005	0.0013	0.0018
(4) Mean	1.0161	1.0460	1.0461	1.0491	1.0539	1.0525
	0.0006	0.0001	0.0001	0.0001	0.0003	0.0006
(5) Mean	1.0130	1.0478	1.0479	1.0513	1.0575	1.0563
	0.0007	0.0002	0.0002	0.0002	0.0005	0.0008
(1') x	1.0906	1.0847	1.0849	1.0906	1.0985	1.0973
	0.0014	0.0004	0.0004	0.0003	0.0006	0.0010
(1') y	1.0128	1.0323	1.0323	1.0342	1.0378	1.0366
	0.0009	0.0001	0.0001	0.0001	0.0003	0.0003
(1') Mean	1.0194	1.0497	1.0497	1.0529	1.0580	1.0567
	0.0018	0.0045	0.0045	0.0049	0.0052	0.0053
(2') x	1.1754	1.1660	1.1664	1.1754	1.1840	1.1890
	0.0021	0.0007	0.0007	0.0006	0.0014	0.0021
(2') y	1.0404	1.0638	1.0638	1.0663	1.0705	1.0705
	0.0009	0.0002	0.0002	0.0002	0.0005	0.0006
(2') Mean	1.0580	1.0977	1.0979	1.1026	1.1084	1.1102
	0.0048	0.0088	0.0088	0.0094	0.0098	0.0102
(3') x	1.4068	1.3967	1.3983	1.4068	1.4187	1.4703
	0.0052	0.0020	0.0021	0.0017	0.0040	0.0067
(3') y	1.1012	1.1430	1.1432	1.1420	1.1528	1.1587
	0.0019	0.0007	0.0007	0.0005	0.0017	0.0028
(3') Mean	1.1565	1.2269	1.2276	1.2300	1.2421	1.2626
	0.0142	0.0219	0.0221	0.0228	0.0229	0.0269

Considering Figure 6a, despite the fact that the *M-tortuosity* values are globally smaller, close to the values of τ_g, it behaves similarly to the state-of-the-art definitions. The values of almost all the plane-based definitions, excepted τ_g, are very similar when compared to τ_g and the *M-tortuosity* (see Table 3). The smaller V_p, the bigger the tortuosity. As mentioned above, $\overline{T_{A(-10,-10)}}$ attests of bigger values of l_σ than $\overline{T_{A(10,-10)}}$, because of short paths promotion. These values of (α_1, α_2) correspond to the minimal and maximal values of the *M-tortuosity*, providing an indication of its range of values. Consequently, the lowest *M-tortuosity* values are obtained for long geodesic paths of source points near p_c, probably shorter than the longest ones, and the biggest *M-tortuosity* are obtained for short geodesic paths of source points near p_c, probably the shortest ones.

Considering Figure 6b, for the plane-based tortuosities, the more heterogeneous the microstructure, the bigger the tortuosity, excepted for the specific case of τ_g which decreases. The behavior of τ_g in Figure 6b is expected. Considering that the volume outside and inside the aggregates is equal, the more heterogeneous the microstructure, the more porous the outside of the aggregates increasing the probability to find a straight path connecting the entry plane to the exit plane. The *M-tortuosity* behaves differently. The long geodesic paths promotion ($\overline{T_{A(10,-10)}}$) leads to a behavior similar to plane-based definitions but with lower values. The short geodesic paths ($\overline{T_{A(-10,-10)}}$) attest of a large diversity of values, seen through l_σ. Indeed, the *M-tortuosity* values of models (1), (4) and (5) are indistinguishable considering the confidence intervals.

Table 4. *M-tortuosities* of microstructures. Average arithmetic *M-tortuosities* as a function of (α_1, α_2), with the corresponding standard deviation std, computed on 40 realizations of each model. Models (1), (2) and (3) assess the impact of volume fraction. Models (4) and (5) assess the impact of heterogeneity. Models (1'), (2') and (3') assess the impact of anisotropy.

	(α_1, α_2)					
	(−10, −10)	(0, −10)	(10, −10)	(−10, 0)	(0, 0)	(10, 0)
Model	l_σ	l_σ	l_σ	l_σ	l_σ	l_σ
(1)	1.0283	1.0102	1.0046	1.0239	1.0085	1.0056
	0.0081	0.0006	0.0005	0.0014	0.0001	0.0002
(2)	1.0526	1.0356	1.0230	1.0589	1.0319	1.0262
	0.0110	0.0012	0.0016	0.0029	0.0004	0.0005
(3)	1.2050	1.1420	1.1160	1.1954	1.1326	1.1231
	0.0437	0.0068	0.0065	0.0076	0.0016	0.0017
(4)	1.0245	1.0119	1.0063	1.0252	1.0100	1.0068
	0.0084	0.0010	0.0007	0.0016	0.0003	0.0002
(5)	1.0339	1.0148	1.0078	1.0286	1.0121	1.0083
	0.0126	0.0012	0.0009	0.0021	0.0003	0.0003
(1')	1.0406	1.0106	1.0011	1.0528	1.0101	1.0023
	0.0089	0.0006	0.0003	0.0027	0.0002	0.0001
(2')	1.0858	1.0355	1.0070	1.1080	1.0339	1.0137
	0.0170	0.0017	0.0010	0.0059	0.0005	0.0003
(3')	1.2463	1.1537	1.0708	1.2935	1.1453	1.0930
	0.0356	0.0056	0.0068	0.0107	0.0016	0.0014

	(α_1,α_2)		
	(−10, −10)	(0, −10)	(10, −10)
Model	l_σ	l_σ	l_σ
(1)	1.0222	1.0081	1.0071
	0.0025	0.0003	0.0005
(2)	1.0524	1.0309	1.0318
	0.0045	0.0005	0.0011
(3)	1.1918	1.1294	1.1294
	0.0112	0.0016	0.0021
(4)	1.0205	1.0094	1.0084
	0.0028	0.0003	0.0005
(5)	1.0285	1.0113	1.0100
	0.0043	0.0004	0.0005
(1')	1.0632	1.0083	1.0027
	0.0072	0.0003	0.0002
(2')	1.1274	1.0293	1.0157
	0.0148	0.0007	0.0008
(3')	1.3446	1.1326	1.0952
	0.0426	0.0024	0.0022

This apparent similarity between models (1) and (4) persists until $\alpha_1 = -1$. For $\alpha_1 \geq 0$ (short paths not promoted) and whatever α_2, the *M-tortuosity* increases with the heterogeneity.

5.3.2 Anisotropic microstructures

As a recall, a compression is simulated in the x direction. Figures 6c and 6d present the anisotropic case with, in Figure 6c the decreasing of V_p and in Figure 6d the analysis of the impacts of (α_1, α_2) (to be compared to Fig. 5b).

Considering Figure 6c, the behaviors are still similar, *i.e.*, increasing of the tortuosity with the decreasing of V_p. In comparison to the isotropic situation, the plane-based tortuosities behave similarly while being bigger (Fig. 6a). The *M-tortuosity* attests of a bigger sensitivity by showing a larger range of values; bigger maximal values ($\overline{T}_{A(-10,10)}$) and smaller minimal values ($\overline{T}_{A(10,-10)}$).

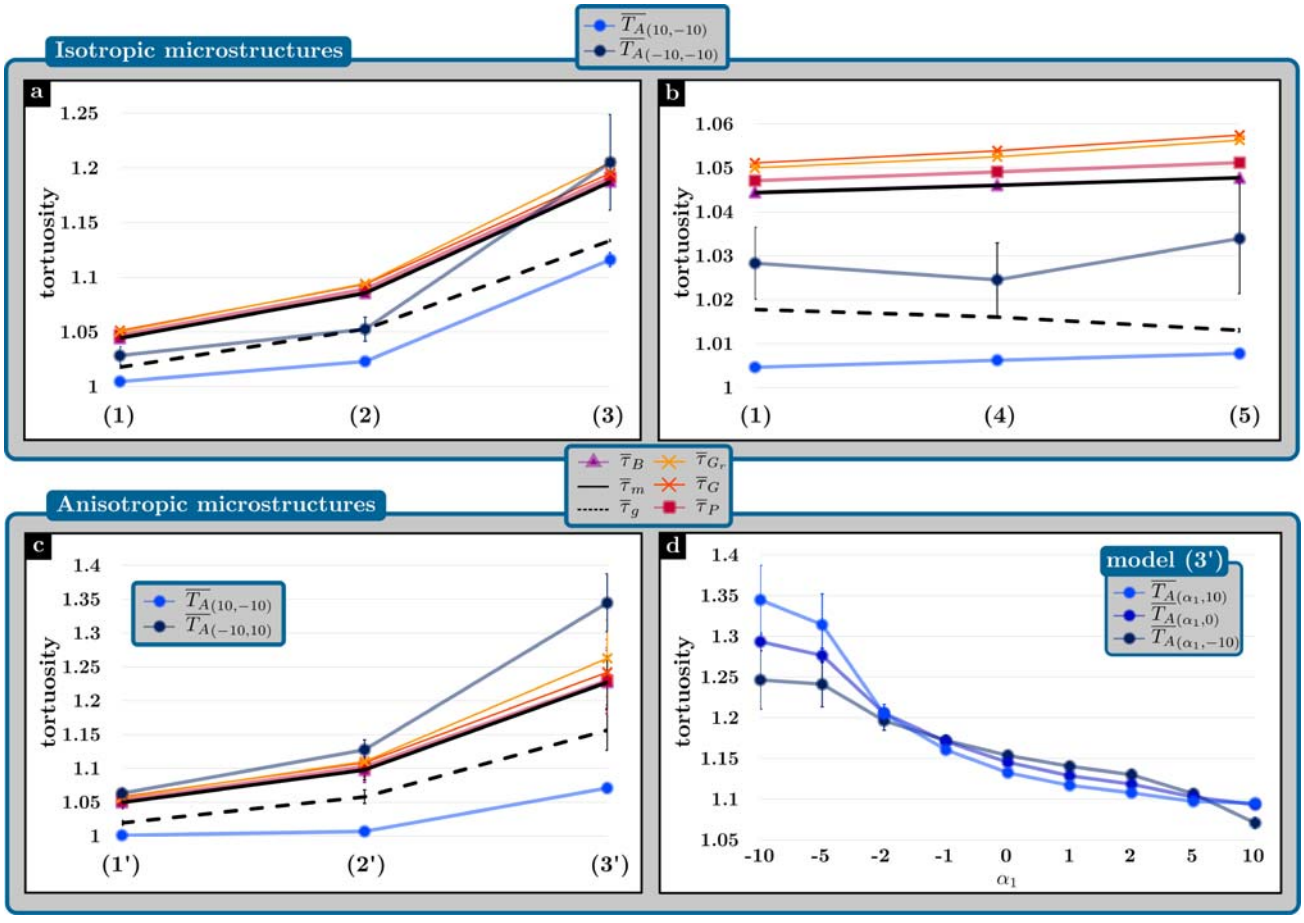

Fig. 6. Tortuosities with respect to porous volume fraction, morphological heterogeneity and structural anisotropy. Average tortuosities with their corresponding confidence intervals l_σ, computed on 40 realizations of each model. (a) Porous volume fraction V_p decreasing with models (1), (2) and (3). (b) Morphological heterogeneity increasing with models (4) and (5). (c)–(d) Structural anisotropy with in (c) decreasing V_p with models (1'), (2') and (3'), and in (d) average arithmetic *M-tortuosity* values of model (3') with a screening of parameters $\alpha_1 = \{-10, -5, -2, -1, 0, 1, 2, 5, 10\}$ and $\alpha_2 = \{-10, 0, 10\}$.

The (α_1, α_2) pair corresponding to the maximal tortuosities is different from the isotropic case. Indeed, the maximal *M-tortuosities* are obtained for the promotion of short geodesic paths far from p_c, probably longer the shortest ones, while the minimal ones correspond to the promotion of long geodesic paths near p_c as in the isotropic situation (Fig. 6a). Figure 6d provides explanations. Indeed the evolution of the arithmetic *M-tortuosity* for the model (3') as a function of $\alpha_1 \in \{-10, -5, -2, -1, 0, 1, 2, 5, 10\}$ and according to $\alpha_2 \in \{-10, 0, 10\}$, behaves similarly to the isotropic situation for long geodesic paths promotion (close to $\alpha_1 = 10$); the classification reversing between the different curves corresponding to the various α_2 values. However, an additional reversing is noticed for α_1 between -2 and -1, when short geodesic paths start to be promoted. Similarly to the plane-based tortuosities which identify anisotropy by the differences between the x, y, z directions (x and y are given in Table 3), this second classification reversing could be a solution for anisotropy detection.

5.3.3 Discriminative power

Discriminative power is the ability of quantitatively distinguishing between two situations, *i.e.*, two distinct microstructures. The tortuosity contrast focuses on small parameters differences by considering the contrast between neighboring models (here multiplied by 1000 to ease the reading). Consequently, the discriminative power is here seen through the absolute value of the tortuosity contrast; the sign provides indications about the tortuosity evolution, *i.e.*, its behavior. The results are presented in Tables 5 and 6; the same parameters selection as above is considered.

Considering the discriminative power and all scenarios, the tortuosity contrasts highlight some differences between the plane-based tortuosities and the *M-tortuosity*. Despite the *M-tortuosity* is inherently complementary to the usual descriptors, some values of (α_1, α_2) allow the *M-tortuosity* to be in the same range of values as the state-of-the-art definitions. For the isotropic and the anisotropic homogeneous

Table 5. Tortuosity contrast and discriminative power (plane-based tortuosities). Tortuosity contrasts, computed on each pair of neighboring models and multiplied by 1000. Models contrasts (2)–(1) and (3)–(2) focus on volume fraction. Models contrasts (4)–(1) and (5)–(4) focus on heterogeneity. Models contrasts (2')–(1') and (3')–(2'), and (1')–(1), (2')–(2) and (3')–(3) focus on anisotropy; two propagating direction are evaluated, x (compression direction) and y (perpendicular direction).

	Tortuosity					
Models	τ_g	τ_m	τ_B	τ_P	τ_G	τ_{G_r}
(2)–(1) Mean	16.7722	19.2918	19.3079	19.7127	19.8148	20.7342
(3)–(2) Mean	37.0333	44.7515	44.8455	43.8383	44.3430	48.0245
(4)–(1) Mean	−0.8235	0.7855	0.7960	0.9559	1.3239	1.2092
(5)–(4) Mean	−1.5124	0.8427	0.8557	1.0286	1.6917	1.7781
(2')–(1') x	29.1309	36.1049	36.1845	37.4475	37.4696	40.1041
(2')–(1') y	13.4701	15.0265	15.0357	15.2992	15.5176	16.1124
(2')–(1') Mean	18.5355	22.3713	22.4062	23.0458	23.2910	24.6905
(3')–(2') x	72.3689	90.0302	90.4532	89.6071	90.1563	105.7989
(3')–(2') y	28.3907	35.8888	35.9602	34.2690	37.0315	39.5332
(3')–(2') Mean	44.5010	55.5838	55.7895	54.6308	56.8537	64.2439
(1')–(1) x	6.9698542	18.9416136	18.9984366	20.3329788	22.0123757	21.9026839
(1')–(1) y	−2.3933944	−5.88022862	−5.88897808	−6.28823676	−6.39779919	−6.48961922
(1')–(1) Mean	0.82760245	2.53647373	2.5502427	2.7526925	3.25508346	3.16580604
(2')–(2) x	20.0463449	35.7749669	35.8928035	38.1020339	40.0873376	41.7567377
(2')–(2) y	−6.44152978	−10.1851369	−10.1993753	−10.7462245	−10.7905948	−11.1304736
(2')–(2) Mean	2.59147916	5.61729475	5.64983032	6.08728922	6.73277598	7.1240219
(3')–(3) x	53.4442072	78.9423319	79.3866642	82.9512547	88.1696935	100.491996
(3')–(3) y	−13.3856754	−18.5636667	−18.6052757	−20.0874668	−18.6192558	−20.1281987
(3')–(3) Mean	10.0713305	16.4756856	16.6203024	16.9045713	19.273502	23.3909106

scenarios, the discriminative power is inversely proportional to V_p. For the isotropic heterogeneous scenario, the discriminative power increases. For the last scenario, comparing isotropic and anisotropic situations at constant V_p, the discriminative power increases as V_p decreases. Moreover, as a global statement, this monotonic evolution of the tortuosity discriminative power seems to tend toward infinity when models tend toward the morphological limit; the percolation threshold ρ of the V_p for the volume fraction based scenarios, isotropic and anisotropic, complete aggregation for heterogeneity based scenario and complete compression for isotropy *vs.* anisotropy scenario. In other words, the discriminative power increases as a function of microstructure parameters, whatever the tortuosity definition or the type of microstructure, among the tortuosity and the models considered.

The above comments about the tortuosities behaviors are underscored by the focus on the contrast sign. Comparing isotropic and anisotropic microstructures at constant V_p (three last lines of Tables 5 and 6), the plan-based tortuosities decrease in the y direction, similarly to the *M-tortuosity* when long geodesic paths are promoted, and increase in the x direction, the one of the compression, similarly to the *M-tortuosity* when short geodesic paths are promoted. Globally, the mean values over the x, y, z directions increase with the anisotropy which have been highlighted in Figures 6a and 6c. The *M-tortuosity* (Table 6) increases similarly for $\alpha_1 < 0$ but starts decreasing at $\alpha_1 = 0$, whatever α_2, meaning that long geodesic paths are less tortuous in average for anisotropic microstructures than for isotropic ones.

5.4 Overall view

Considering all scenarios, the plane-based tortuosities are equivalent, excepted τ_g which is always smaller and the only tortuosity to decrease in the heterogenity scenario. On closer inspection, τ_B is almost equal to the classical τ_m, τ_P is a little bit bigger than τ_B while τ_G and τ_{G_r} are generally the biggest; τ_{G_r} is bigger than τ_G except for the heterogeneity scenario. In the anisotropic scenario, the differences between the tortuosity values according to the direction is a way to detect anisotropy in a microstructure. In this case, considering tortuosity behaviors as functions of V_p, there is a contradiction for the plane-based definitions; in the x direction (compression direction) the tortuosities are bigger than the isotropic case, in the y direction the tortuosities are smaller. Globally, according to the mean tortuosity, the anisotropy induces an increasing of the tortuosity.

Let consider the *M-tortuosity* with the arithmetic definition. Globally, the short geodesic paths makes increase the tortuosity (α_1 tends toward minus infinity), while increasing the uncertainty about the mean value. For isotropic scenarios (Figs. 6a and 6b), it provides smaller tortuosity values than the other plane-based definitions, excepted for the model (3). For anisotropic scenario, the situation is different. The power factor α_1 provides a certain control of the

Table 6. Tortuosity contrast and discriminative power (*M-tortuosity*). *M-tortuosity* contrasts as a function of (α_1, α_2), computed on each pair of neighboring models and multiplied by 1000. Models contrasts (2)–(1) and (3)–(2) focus on volume fraction. Models contrasts (4)–(1) and (5)–(4) focus on heterogeneity. Models contrasts (2')–(1') and (3')–(2'), and (1')–(1), (2')–(2) and (3')–(3) focus on anisotropy.

	(α_1, α_2)					
Models	(−10, −10)	(0, −10)	(10, −10)	(−10, 0)	(0, 0)	(10, 0)
(2)–(1)	11.6585	12.4112	9.0540	16.8155	11.4334	10.1831
(3)–(2)	67.5180	48.8562	43.4857	60.5600	46.5211	45.0741
(4)–(1)	−1.8375	0.8327	0.8099	0.6516	0.7427	0.6364
(5)–(4)	4.5627	1.4065	0.7480	1.6446	0.9999	0.7313
(2')–(1')	21.2390	12.1347	2.9192	25.5741	11.6728	5.6274
(3')–(2')	68.8360	53.9952	30.7437	77.2097	51.1185	37.6858
(1')–(1)	5.9563	0.2122	−1.7625	13.9149	0.7468	−1.6181
(2')–(2)	15.5383	−0.0644	−7.8974	22.6745	0.9862	−6.1740
(3')–(3)	16.8621	5.0881	−20.6544	39.3874	5.5946	−13.5743

	(α_1, α_2)		
Models	(−10, −10)	(0, −10)	(10, −10)
(2)–(1)	14.5242	11.1650	12.0952
(3)–(2)	62.1177	45.6178	45.1820
(4)–(1)	−0.8518	0.6512	0.6547
(5)–(4)	3.8986	0.9231	0.7583
(2')–(1')	29.3014	10.3329	6.4218
(3')–(2')	87.8860	47.7690	37.6804
(1')–(1)	19.6453	0.0638	−2.2011
(2')–(2)	34.4187	−0.7685	−7.8748
(3')–(3)	60.2747	1.3874	−15.3884

sensitivity to geodesic paths length. This is a complementary insight over the whole microstructure. Moreover, beside this first benefit, the *M-tortuosity* probes the microstructures in random directions, not only the x, y, z ones, and succeeds in detecting the anisotropy (Fig. 6d). Consequently, the *M-tortuosity* reveals to be a good candidate to characterize thoroughly complex microstructures where propagation direction is delicate to impose. Moreover, the choices of (α_1, α_2) could be motivated by the application, if the local diffusion is to be analyzed as in [25].

Finally, if the purpose is to analyze microstructures using a unique scalar value, it is of interest to identify the values of (α_1, α_2) to simulate the state-of-the-art definitions in applications they do not fit. As the discriminative power of the *M-tortuosity* is often larger than the usual definitions, no perfect matching is reachable. In the isotropic scenarios, $\alpha_1 = -10$ leads to closer tortuosity values to the plane-based ones. Still in the isotropic scenarios, for the specific case of τ_g, the closest curves are obtained for α_1 around -2 for the volume fraction scenario. For the heterogeneity one, the behaviors are too different; $\alpha_1 \geq 0$ ensures the *M-tortuosity* to increase. The value of α_2 impacts less the final result, which is expected with isotropic microstructures. Nonetheless, it seems that when α_2 tends toward minus infinity the tortuosity increases but large values of l_σ add uncertainty in the average value. Indeed, α_2 has an influence over the confidence interval; in the volume fraction scenario as well as in the heterogeneity one, $\alpha_2 = 0$ provides the lowest l_σ values. In the anisotropic situation, the range of *M-tortuosity* values encompasses the state-of-the-art tortuosity values. The closest values are obtained for $\alpha_1 = \alpha_2 = -10$. For the specific case of τ_g, the closest curves are obtained for $\alpha_1 = -1$, whatever α_2.

6 Conclusion

Based on a stochastic process, the *M-tortuosity* fits with the characterization of complex microstructures where propagation directions are delicate to impose, such as irregular piece of materials or atypical contexts. The extension presented in this work provides versatility through additional parameters making explicit the consideration of percolation while giving the opportunity to the user to adapt the characterization to the application. A brief review of morphological visions of tortuosity is presented and the *M-tortuosity* is compared to these state-of-the-art descriptors.

The new parameter α_1 added to the original *M-tortuosity* definition provides a certain sensitivity to geodesic paths lengths, allowing to promote long or short geodesic paths. α_2 promotes or inhibits eccentricity in microstructure probing. The other parameters, named ρ, embed percolation to get a proper disconnection and isolation insensitivity, one ofthe distinctions with the state-of-the-art. Moreover, the

M-tortuosity probes the microstructures in random directions, not only the x, y, z ones, particularly adapted to applicative situations where propagation direction is undefined or if only local diffusion is to be quantified. The *M-tortuosity* is compared to some state-of-the-art definitions in three specific situations thanks to Boolean models. The tortuosity behavior with respect to porous volume fraction, morphological heterogeneity and structural anisotropy is evaluated.

As a result, the *M-tortuosity* behavior is equivalent to the state-of-the-art definitions while being inherently complementary thanks to the new parameters. Globally, the short geodesic paths promotion ($\alpha_1 < 0$) leads to an increase in tortuosity, contrary to the long geodesic paths promotion. In the isotropic scenario, the *M-tortuosity* behaves similarly to the plan-based tortuosities but its values are smaller. However, while the anisotropy does not affect the behavioral aspect, the *M-tortuosity* sensivity leads to a larger range of values, encompassing the state-of-the-art tortuosities. The optimal values of (α_1, α_2) to get closer to the plan-based tortuosities are discussed. The *M-tortuosity* is a potential candidate to replace these definitions in situations where they are not adapted to and used in diffusion and conductivity analyses. Moreover, one of the advantages of the *M-tortuosity* relies in the microstructure characterization as a function of the parameters (α_1, α_2), allowing, among other things, to detect anisotropy without imposed propagation direction.

These statements are supported by the discriminative power analysis, based on contrast in tortuosity values of pairs of neighboring models. This highlights once again the similarity of the *M-tortuosity* to the classical definitions considering isotropic microstructures while providing additional details about tortuosity behavior at different scales, especially in the heterogeneity case. Last but not least, anisotropic microstructures point out the differences to the classical definitions. This specific situation of structural anisotropy highlights the contradiction in tortuosity behaviors considering plane-based tortuosities; tortuosity increases or decreases with anisotropy according to the propagation direction. The mean value of the x, y, z directions is considered for comparison with the *M-tortuosity*. Considering the *M-tortuosity* and the standard tortuosties, the detection of the anisotropy is connected to how it impacts the tortuosity according to the length of the geodesic path. The anisotropy leads to increase the tortuosity of short geodesic paths, similarly to its impact in the x direction (compression direction), and to decrease the tortuosity of long geodesic paths, similarly to its impact in the y or z directions.

The versatility of the *M-tortuosity* relies on the various operators it could provide, as demonstrated in [15, 25] which is now enriched by parameters allowing to adapt the computations to the applications. In the future, two main points will be investigated. The first one is the heterogeneity case in the results and discussion section, which points out certain limitations of considering only scalar values to represent the tortuosity of complex microstructures. In this case, a dimension adapted to the required description using 3D maps, curves or histograms could turn the *M-tortuosity* a manyfold tortuosity. The second point concerns its use on real microstructure samples as the one of Figure 1.

The *M-tortuosity* and the state-of-the-art tortuosities discussed in this article are freely available in [35].

References

1 Adler P.M. (1992) *Porous media: geometry and transports*, Butterworth-Heineman, Boston, MA, p. 544.
2 Dullien F.A.L. (1979) *Porous media: fluid transport and pore structure*, Academic press.
3 Raybaud P., Toulhoat H. (2013) *Catalysis by transition metal sulphides: From molecular theory to industrial application*, Editions Technip.
4 Carman P.C. (1937) Fluid flow through granular beds, *Trans. Inst. Chem. Eng.* **15**, 150–166.
5 Clennell M.B. (1997) Tortuosity: a guide through the maze, *Geol. Soc. Spec. Publ.* **122**, 1, 299–344.
6 Fu J., Thomas H.R., Li C. (2021) Tortuosity of porous media: image analysis and physical simulation, *Earth-Sci. Rev.* **212**, 103439.
7 Ghanbarian B., Hunt A.G., Ewing R.P., Sahimi M. (2013) Tortuosity in porous media: a critical review, *Soil Sci. Soc. Am. J.* **77**, 5, 1461–1477.
8 Bini F., Pica A., Marinozzi A., Marinozzi F. (2019) A 3D model of the effect of tortuosity and constrictivity on the diffusion in mineralized collagen fibril, *Sci. Rep. UK* **9**, 1, 2658.
9 Van Brakel J., Heertjes P.M. (1974) Analysis of diffusion in macroporous media in terms of a porosity, a tortuosity and a constrictivity factor, *Int. J. Heat Mass Tranf.* **17**, 9, 1093–1103.
10 Balberg I., Anderson C.H., Alexander S., Wagner N. (1984) Excluded volume and its relation to the onset of percolation, *Phys. Rev. B* **30**, 7, 3933.
11 Jouannot-Chesney P., Jernot J.-P., Lantuéjoul C. (2017) Percolation transition and topology, *Image Anal. Stereol.* **36**, 95–103.
12 Petersen E.E. (1958) Diffusion in a pore of varying cross section, *AIChE J.* **4**, 3, 343–345.
13 Tran V.-D., Moreaud M., Thiébaut E., Denis L., Becker J.-M. (2014) Inverse problem approach for the alignment of electron tomographic series, *Oil Gas Sci. Technol. Rev. IFP Energies Nouvelles* **69**, 2, 279–291.
14 Chaniot J., Moreaud M., Sorbier L., Becker J.-M., Fournel T. (2019) Tortuosimetric operator for complex porous media characterization, *Image Anal. Stereol.* **38**, 1, 25–41.
15 Chaniot J., Moreaud M., Sorbier L., Jeulin D., Becker J.-M., Fournel T. (2020) Heterogeneity assessment based on average variations of morphological tortuosity for complex porous structures characterization, *Image Anal. Stereol.* **39**, 2, 111–128.
16 Stenzel O., Pecho O., Holzer L., Neumann M., Schmidt V. (2016) Predicting effective conductivities based on geometric microstructure characteristics, *AIChE J.* **62**, 5, 1834–1843.
17 Lantuéjoul C., Beucher S. (1981) On the use of the geodesic metric in image analysis, *J. Microsc.* **121**, 1, 39–49.
18 Decker L., Jeulin D., Tovena I. (1998) 3D morphological analysis of the connectivity of a porous medium, *Acta Stereol.* **17**, 1.
19 Saha P.K., Borgefors G., di Baja G.S. (2016) A survey on skeletonization algorithms and their applications, *Pattern Recogn. Lett.* **76**, 3–12.
20 Peyrega C., Jeulin D. (2013) Estimation of tortuosity and reconstruction of geodesic paths in 3D, *Image Anal. Stereol.* **32**, 1, 27–43.

21 Berrocal C.G., Löfgren I., Lundgren K., Görander N., Halldén C. (2016) Characterisation of bending cracks in R/FRC using image analysis, *Cement Concrete Res.* **90**, 104–116.

22 Gommes C.J., Bons A.-J., Blacher S., Dunsmuir J.H., Tsou A.H. (2009) Practical methods for measuring the tortuosity of porous materials from binary or gray-tone tomographic reconstructions, *AIChE J.* **55**, 8, 2000–2012.

23 Boudreau B.P. (1996) The diffusive tortuosity of fine-grained unlithified sediments, *Geochim. Cosmochim. Acta* **60**, 16, 3139–3142.

24 Moreaud M., Celse B., Tihay F. (2008) Analysis of the accessibility of macroporous alumino-silicate using 3D-TEM images, in: Vol. **8** of *Proceedings of Materials Science & Technology 2008 Conference and Exhibition: MS&T*, pp. 1153–1164.

25 Batista A.T.F., Baaziz W., Taleb A.-L., Chaniot J., Moreaud M., Legens C., Aguilar-Tapia A., Proux O., Hazemann J.-L., Diehl F., Chizallet C., Gay A.-S., Ersen O., Raybaud P. (2020) Atomic scale insight into the formation, size and location of platinum nanoparticles supported on γ-alumina, *ACS Catal.* **10**, 7, 4193–4204.

26 Caflisch R.E. (1998) Monte Carlo and quasi-Monte Carlo methods, *Acta Numer.* **7**, 1–49.

27 Hammoumi A., Moreaud M., Jolimaitre E., Chevalier T., Novikov A., Klotz M. (2021) Graph-based M-tortuosity estimation, in: *Discrete Geometry and Mathematical Morphology*, J. Lindblad, F. Malmberg, N. Sladoje (eds), Lecture Notes in Computer Science, Springer, Cham, pp. 416–428.

28 Chaniot J., Moreaud M., Sorbier L., Becker J.-M., Fournel T. (2022) Scalable morphological accessibility of complex microstructures, *Comp. Mater. Sci.* **203**, 111062.

29 Allard J.F., Castagnede B., Henry M., Lauriks W. (1994) Evaluation of tortuosity in acoustic porous materials saturated by air, *Rev. Sci. Instrum.* **65**, 3, 754–755.

30 Johnson D.L., Plona T.J., Scala C., Pasierb F., Kojima H. (1982) Tortuosity and acoustic slow waves, *Phys. Rev. Lett.* **49**, 25, 1840.

31 Kingman J.F.C. (1992) *Poisson processes, volume 3 of Oxford studies in probability*, Clarendon Press, Oxford Science Publications.

32 Jeulin D. (2012) Morphology and effective properties of multi-scale random sets: A review, *C.R. Mecanique* **340**, 4–5, 219–229.

33 Moreaud M., Chaniot J., Fournel T., Becker J.-M., Sorbier L. (2018) Multi-scale stochastic morphological models for 3D complex microstructures, in: *2018 17th Workshop on Information Optics (WIO)*, IEEE, Quebec, Canada, pp. 1–3.

34 Wang H., Pietrasanta A., Jeulin D., Willot F., Faessel M., Sorbier L., Moreaud M. (2015) Modelling mesoporous alumina microstructure with 3D random models of platelets, *J. Microsc.* **260**, 3, 287–301.

35 plug im! (2018) *An open access and customizable software for signal and image processing.* Available at https://www.plugim.fr.

36 Chiu S.N., Stoyan D., Kendall W.S., Mecke J. (2013) *Stochastic geometry and its applications*, John Wiley & Sons.